 doi:10.20944/preprints202202.0360.v1

Effect of kinematic algorithm selection on the conceptual design of orbitally delivered vehicles

David Cole[1], Timothy Sands[2,*]

[1] Department of Mechanical and Aerospace Engineering, Naval Postgraduate School; david.cole@nps.edu
[2] Sibley School of Mechanical and Aerospace Engineering; Cornell University; tas297@cornell.edu

Abstract: A particular challenge in the conceptual design of direct-from orbit delivery systems is the seemingly well-known kinematics retain fallacies whose efficacies are reduced over great distances. Rotation about the local wing of an aerospace vehicle is almost never the pitch angle, yet modern application of kinematics often assumes such (with accompanying angular error). The same assertion is usually true about the nature of roll and yaw angles. Expressing motion in coordinates of rotating reference frames necessitates transformation between reference frames, and one such transformation is embodied in the Direction Cosine Matrices (DCM) formed by a sequence of three successive frame rotations. One of two ubiquitous sequences of three rotations used to construct the DCM involves first a rotation around the inertial z-axis, then intermediate y-axis, then finally about the body's x-axis; a sequence commonly called the "aerospace sequence" or the a "3-2-1 rotation sequence". The second ubiquitous sequence is the so-called "orbital sequence" or "3-1-3 rotation sequence" with rotations about the inertial z axis first, then about the intermediate x-axis, then finally about the body z-axis. This manuscript evaluates which sequence is the most advantageous for an object starting in space and then travels through the atmosphere to a target on the Earth's surface. Six degrees of freedom of vehicle motion were simulated starting in orbit with a given thrust and commanded maneuver. The simulation performs all twelve possible rotation sequences (transforming inertial coordinates to body coordinates) with comparison by computational burden and error representing rotations about body axes (roll, pitch, and yaw respectively). Simulation precision is validated using the quaternion normalization condition indicating near machine precision (0.9×10^{-1}) and reveals the so-called 132 rotation is the most accurate with an average error of 0.14° and a computational time of 0.013 seconds: resulting in a 97.95% increase in accuracy over the so-called 321 rotation and a 99.84% increase over the so-called 313 rotation.

Keywords: GNC system design; design and analysis of orbit/attitude determination and control systems; motion planning; guidance; control; trajectory planning; conceptual design; kinematics; direction cosine matrix; DCM; 6 Degrees of Freedom; 6 DOF

1. Introduction

The study of dynamic motion comprises kinetics (the study of forces in action) and kinematics (properties of motion without reference to forces). Formal study of kinematics in modern times stems from the original works of Swiss mathematician Leonhard Euler in 1775 [1]. Sir William Thomson (Lord Kelvin) and physicist Peter Guthrie Tait [2] demonstrated the centrality of energy conservation to systems of dynamic movement. The greater part of *Theoretische Kinematik* by Professor Franz Reuleaux was published in English in 1876 as [3] becoming a regular part of curricula in Russia, Italy, and the United States. The book compiled practices of engineers who had theretofore been left to work out the subject for themselves. By 1898 Thomas Wallace Wright compiled a treatise [4] on the topics designed for mathematics no more complicated than elementary principles of geometry, trigonometry, and the calculus (for those desiring a more compact form). Seeking to unify the field, German British chemist John Theodore Merz published a history of European thought in the nineteenth century in 1903 [5]. It is noteworthy that 1903 is the

 doi:10.20944/preprints202202.0360.v1

same year of the first heavier-than-air flight of an airplane by the Wright Brothers in North Carolina, USA.

The field of kinematics had matured for more than a century as a philosophy and a field of engineering at the time of the advent of (un-instrumented) aircraft flight.

The following year, Englishman Sir Edmund Taylor Whittaker sought to give justice to the earliest work of Hamilton, Rodrigues, and Chasle in his publication of four editions [6-9]. While Sir Whittaker's treatise was an attempt at a philosophical treatment, Irving Porter Church published a guidebook focused on engineering [10] in 1908. Thirteen years after his earlier work, Thomas Wallace Wright [11] refreshed his attempt to treat the topics with basic mathematics. Seemingly seeking to lower the mathematical level even further to the level of ordinary geometry, in 1913 German mathematician Christian Hugo Eduard Study published reference [12]. In 1918, Andrew Gray published [13] where he emphasized the key feature of dynamics (kinetics and kinematics) resided in kinematics. Years later in 1954, Clifford Truesdell echoed the sentiment [14], "I cannot too strongly urge that a kinematical result is a result valid forever, no matter how time and fashion may change the "laws" of physics." In 1967 English author G.C. Fox reaffirmed [15], "It is my belief that students have difficulty with mechanics because of an inadequate knowledge of kinematics."

Proceeding decades solidified the nascent notions of dynamics until a new notion arose from Kane [17,18] in the late 1950's elaborating the so-called D'Alembert's version of Lagrange's equation, principally focused on kinetics. With the burgeoning computational abilities of the 1960's Fang leveraged these abilities to establish a mathematical simulation model for rigid body rotational kinematics [19]. Henderson [20-21] expressed the formal instantiation of kinematic relationships between rotational sequences, four-dimensional quaternions, and direction cosine matrices in the late 1970's.

From this distinguished lineage, terminology has converged to refer to sequential rotation sequences, with two favored sequences called 1) aerospace sequences about non-repeating axes (also referred to as "Tait-Bryan angles"), while 2) the orbital sequence has an axis-type repeated in the rotation sequence (also referred to as "proper Euler angles").

Is the ubiquitous aerospace sequence (3-2-1) the best rotation sequence? Instead, is the orbital sequence (3-1-3) better? What about the other ten options to transform inertial coordinates to body coordinates? In 2018, Smeresky and Rizzo [22] highlighted the ubiquitously accepted yaw angle in the standard "3-2-1" aerospace sequence *does not* accurately represent rotation about a rigid body's z-axis, and furthermore the pitch angle *does not* accurately represent rotation about a rigid body's y-axis, while *only* the roll angle accurately represents rotation about a rigid body's x-axis. Smeresky and Rizzo motivate the novel innovations presented in this manuscript.

Evaluation of all twelve options will be driven by two figures of merit. Mean and standard deviations of *representation* errors indicating how well each rotation sequence represents true roll, pitch, and yaw angles (ASIDE: The treatment of representation errors distinguishes this work from Smeresky, et. al, [22] who merely examined the resulting tracking errors, but not the absolute representation errors.) Computation burden represented by calculation-time to reveal relative numerical superiority (ASIDE: Calculation-time is also distinguished from Smeresky, et. al, [22] who merely examined the end-to-end simulation run-time using *tic and toc* commands in MATLAB/SIMULINK, while this manuscript highlights the precise execution time of the rotation sequence choice itself.)

Analysis and results demonstrate the fact that aerospace sequence and its reverse sequence (the 123) result in disparate errors and computation time, with the former being relatively superior. Furthermore, the 123 rotation was significantly slower than all the other rotations. Secondly, symmetric rotation sequences were on average slower than the non-symmetric sequences, despite the same mathematical process and number of steps to solve for the Euler Angles. Lastly, the fastest non-symmetric rotation was the 321 and the fastest symmetric was the 232, slightly faster than the 121 sequence. Considering all direction cosine matrix (DCM) rotation sequence options, the 232 rotation was the fastest.

 doi:10.20944/preprints202202.0360.v1

1.1. Broad context and proposed innovations

This manuscript describes three-dimensional (rotational and translational) motion with six degrees of freedom when applied to a vehicle delivered from geostationary orbit. Due to size constraints in modern vehicles and to minimize necessary computing power, efficient schemes are desired to provide vehicle guidance. Determining the most accurate and computationally efficient rotation sequence is, therefore, essential to producing an effective space delivered weapon.

This research simulates a vehicle launched from orbit with limited computing power. Proposed innovations include:

1. Identification of most accurate rotation sequence, where accuracy is evaluated based on ability to correctly represent rotations about bode axes (the paradigm expected by a pilot).
2. Identification of the options with advantageous computational requirements.

Section two describes the materials and the methods used to reveal the results presented in section 3. The discussion in section 4 will present results in broadest possible terms.

2. Materials and Methods

For kinetics this manuscript will discuss the use of Newton's and Euler's principles and specifically how they combine to form Chasle's theorem in order to form a direct line to explaining the six degrees of freedom in kinetics. Direction cosines and the matrices they form, or quaternions, describe the body of an object in terms of a predefined axis.

2.1 Kinetics of rotational motion

In accordance with Euler's equations of motion, the sums of externally applied torques will angularly accelerate a proportional mass moment of inertia as depicted in Equation 1, where τ is torque, J is the rotation tensor, and ω is the angular velocity.

$$\tau|_n = J\alpha_n \rightarrow \tau = J\dot{\omega} + \omega \times J\omega \tag{1}$$

2.2 Kinetics of translational motion

Similarly, an object of a defined mass will accelerate proportionally to the sum of forces acting on that mass in accordance with Newton's second law as depicted in Equation 2 where F is the force, m is the defined mass, a is the acceleration, ω is angular velocity, r′ is the position vector, and v′ is velocity vector.

$$F = ma + m\frac{d\omega}{dt} \times r' + 2m\omega \times v' + m\omega \times (\omega \times r') \tag{2}$$

Newton's law applies in the inertial frame and allows us to express our results in a set of coordinates in another defined frame of reference.

2.3 Kinetics of disturbance forces and torques

Disturbance forces and torques act on a body in accordance with equations (1) and (2) and are accounted for within the Simulink model for simulation found in Appendix (A).

Preprints (www.preprints.org) | NOT PEER-REVIEWED | Posted: 28 February 2022 doi:10.20944/preprints202202.0360.v1

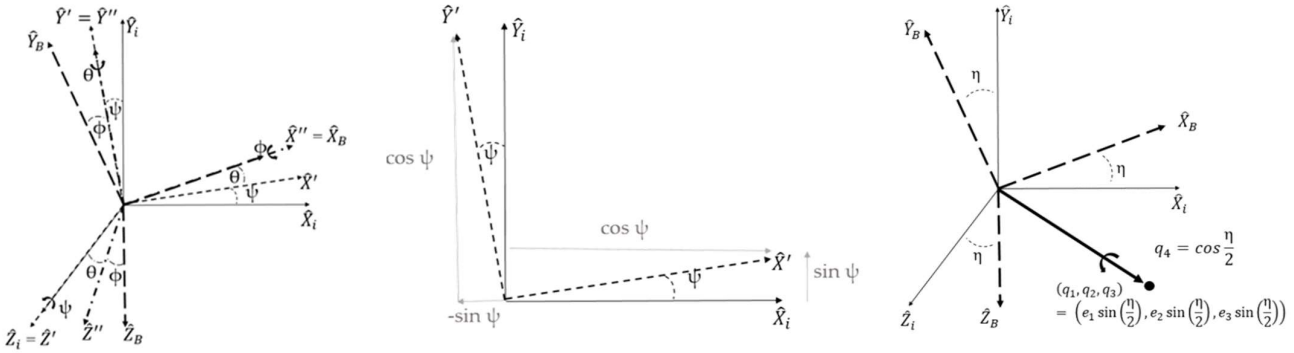

(**a**) (**b**) (**c**)

Figure 1. 1a is a depiction of three-dimensional comparison of the body frame to the inertial frame through prime axes by the Euler angles pitch (θ), roll (ϕ) and yaw (ψ). 1b depicts determining the sign value of each sine or cosine for direction cosine matrix (DCM) of rotating about the Z_i axis. 1c depicts a rotation using a quaternion to directly compare the inertial frame to the body frame by mathematically rotating around a 4th axis, defined in relation to the eigenvector, by the angle η.

2.4 Kinematics of motion in three degrees

By utilizing direction cosines, we are able to take a set of coordinates relative to the non-rotating inertial frame and express them in terms of the body frame to account for motion in all three degrees as depicted in Figure 1, where all lines are unit vectors and the thin solid line represents the non-rotating inertial frame and each dash line increasing in weight indicates the first prime, second prime and finally the body frame respectively.

The DCM is labeled in the order the mathematical calculations are solved, right to left in accordance with algebraic multiplication rules to pre-multiply the total transformation matrix. Equation (3) represents the three mathematical calculations for a "3-2-1" rotation and is then multiplied to generate the total DCM in Equation (4).

$$\begin{Bmatrix} X_B \\ Y_B \\ Z_B \end{Bmatrix} = \underbrace{\begin{bmatrix} 1 & 0 & 0 \\ 0 & \cos(\Phi) & \sin(\Phi) \\ 0 & -\sin(\Phi) & \cos(\Phi) \end{bmatrix}}_{1\ rotation\ (about\ Z''=Z_B)} \underbrace{\begin{bmatrix} \cos(\Theta) & 0 & -\sin(\Theta) \\ 0 & 1 & 0 \\ \sin(\Theta) & 0 & \cos(\Theta) \end{bmatrix}}_{2\ rotation\ (about\ Y')} \underbrace{\begin{bmatrix} \cos(\psi) & \sin(\psi) & 0 \\ -\sin(\psi) & \cos(\psi) & 0 \\ 0 & 0 & 1 \end{bmatrix}}_{3\ Rotation\ (about\ Z_i)} \begin{Bmatrix} X_i \\ Y_i \\ Z_i \end{Bmatrix}, \quad (3)$$

$$\begin{Bmatrix} X_B \\ Y_B \\ Z_B \end{Bmatrix} = \begin{bmatrix} \cos(\Theta)\cos(\psi) & \cos(\Theta)\sin(\psi) & -\sin(\Theta) \\ \sin(\Phi)\sin(\Theta)\cos(\psi) - \cos(\Phi)\sin(\psi) & \sin(\Phi)\sin(\Theta)\sin(\psi) + \cos(\Phi)\cos(\psi) & \sin(\Phi)\cos(\Theta) \\ \cos(\Phi)\sin(\Theta)\cos(\psi) + \sin(\Phi)\sin(\psi) & \cos(\Phi)\sin(\Theta)\sin(\psi) - \sin(\Phi)\cos(\psi) & \cos(\Phi)\cos(\Theta) \end{bmatrix} \begin{Bmatrix} X_i \\ Y_i \\ Z_i \end{Bmatrix} \quad (4)$$

A mathematical problem arising from the DCM is the inability to pull values directly from the matrix due to quadrant ambiguity presented by the law of sines and cosines. To solve the quadrant ambiguity problem, you have to pluck out the portions of the DCM that allow you to use the atan2 function to solve for a specific angle by cancelling out other portions, as shown in Equation 5 in which the atan2 function distinguishes between the four standard reference quadrants.

$$tan^{-1}\left(\frac{[DCM](1,2)}{[DCM](1,1)}\right) = atan2\left(\frac{cos\theta sin\psi}{cos\theta cos\psi}\right) = \psi \quad (5)$$

An additional mathematical error from the law of sines and cosines is singularities in the DCM from solutions equaling 1/0. Lastly, the DCM, based on the chosen order of rotation, results in errors in the final result with only the "last" rotation having zero error due to being the only rotation about the body axis. To account for zero error in all three Euler angles, an additional rotation needs to be completed for each angle in the "last" position.

Preprints (www.preprints.org) | NOT PEER-REVIEWED | Posted: 28 February 2022 doi:10.20944/preprints202202.0360.v1

One way to remove the singularity problem presented by DCMs is to use the quaternion where the three-dimensional rotation is executed around a 4th axis; a scaled, stretched and normalized eigenvector, instead of the three standard axes. This requires induction of three imaginary axes of motion as opposed to the standard inertial frame and is shown in Figure (1c) and Equation (6) where q represents the different values of the quaternion and η is the angle that allows a single rotation [1,2]. The quaternion works so long as we enforce the quaternion normalization condition shown in Equation (6). Specifically, Equation (6) shows a direct comparison to the DCM shown in Equation (4).

$$\begin{Bmatrix} X_B \\ Y_B \\ Z_B \end{Bmatrix} = \underbrace{[DCM]\begin{Bmatrix} X_i \\ Y_i \\ Z_i \end{Bmatrix}}_{Equation\ (4)} = \underbrace{\begin{bmatrix} 1-2(q_2^2+q_3^2) & 2(q_1q_2+q_3q_4) & 2(q_1q_3+q_2q_4) \\ 2(q_1q_2+q_3q_4) & 1-2(q_1^2+q_3^2) & 2(q_2q_3+q_1q_4) \\ 2(q_1q_3+q_2q_4) & 2(q_2q_3+q_1q_4) & 1-2(q_1^2+q_2^2) \end{bmatrix}}_{Quaternion\ Matrix} \begin{Bmatrix} X_i \\ Y_i \\ Z_i \end{Bmatrix} \begin{matrix} So \\ Long \\ As \end{matrix} \underbrace{q^Tq+q_4^2 = q_1^2+q_2^2+q_3^2+q_4^2 = 1}_{Quaterion\ Normaliztion\ Condition} \quad (6)$$

2.5. Guidance of motion in three degrees

The guidance of objects is known as the outer loop function and generates commands for the inner loop discussed in section 2.5 by accounting for three degrees of freedom of translational motion governed by Newton's 2nd Law expressed in Equation (2).

2.6. Control of motion in three degrees

Control of motion is accomplished in the inner loop function by determining the attitude and controls in three degrees of freedom of rotational motion governed by Euler's law expressed in Equation (1) and is constantly affected by the guidance discussed in section 2.5.

2.8. Decoupling nonlinear coupled motion

Due to the transport theorem, ω couples the three degrees of freedom of translational and rotational motion. Additionally, equations (1) and (2) are internally coupled within the inertia matrix with ω, causing motion in all three degrees with inputs to only one. A non-linear decoupling controller is placed in a feedback control, or a desired output is placed in a feed forward control, to decouple the nonlinear couple motion as displayed in equation (7) where u is the controller and ω_d is the desired output angular velocity.

$$T = u - \underbrace{(\omega \times J\omega)}_{\substack{non-linear \\ decopuling\ controller}} = u + \underbrace{\omega_d + J\omega_d}_{\substack{Desired\ output \\ for\ feed\ forward}} \quad (7)$$

2.9. Summary

By using Newton's and Euler's equations and invoking Chasle's method, we are able to express six degrees of freedom for a three-dimensional movement of an object. DCMs are then used to describe the position of a body in terms of a defined axes, with quaternions used to eliminate singularities and validate the DCM. From these equations we pull out the true Euler angles.

3. Results

3.1. Simulation configurations and accuracy

The simulation was run using multiple Matlab Simulink solvers in order to determine the accuracy of the simulation as demonstrated in Figure (2).

Preprints (www.preprints.org) | NOT PEER-REVIEWED | Posted: 28 February 2022 doi:10.20944/preprints202202.0360.v1

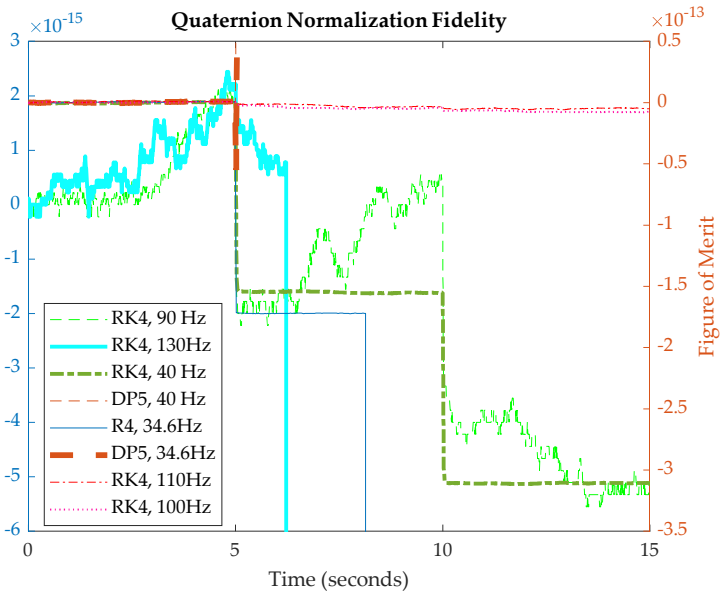

(a)

Table 1. Quaternion normalization errors for different solver schemes

Solver	Solver Type	Frequency (Hz)	Max Error
ode4	Runge-Kutta	34.6	$1.6x10^{-10}$
ode5	Dormand-Prince	34.6	$1.1x10^{-12}$
ode5	Dormand-Prince	40	$1.7x10^{-9}$
ode4	Dormand-Prince	40	$3.1x10^{-13}$
Auto	Auto Select	FAILED	FAILED
ode4	Runge-Kutta	90	$2.1x10^{-15}$
ode4	Runge-Kutta	110	$1.4x10^{-15}$
ode4	Runge-Kutta	130	$1.4x10^{-11}$
ode4	**Runge-Kutta**	**100**	**$0.9\ x10^{-15}$**

[1] Runge-Kutta (ode4) with 100Hz was selected

(b)

Figure 2. Comparison of quaternion normalizations (on the ordinate) for different step sizes and solver schemes. Maximum error for each step size and associated solver are displayed in Table (1)

Using the quaternion normalization condition, the simulation was verified to be accurate to near machine precision in the case of input to a single Euler angle while accounting for six degrees of freedom. For commanded Pitch, Roll and Yaw simultaneously, best precision was found to be $4.8x10^{-11}$ using the ode4 solver with a frequency of 117Hz.

3.2. Dynamics of motion in six degrees

The only change between tests was the order of the mathematical rotation conducted in the DCM in order to validate the accuracy and computation required for each and allow a direct comparison.

3.2.1 Kinetics of rotational motion

The simulation ran in accordance with Euler's equations of motion accounting for the changing angular velocities and accelerations found with a falling and rotating object, while accounting for the rotation of the earth under the falling vehicle.

3.2.2 Kinetics of translational motion

With mass remaining constant, the simulation runs in accordance with Newton's second law. The simulation starts in a geosynchronous orbit with less velocity than required to maintain orbit. This initial condition, coupled with the commanded inputs, immediately initiates a dive towards the earth with a constant thrust along the X_{Body} axis.

3.2.3 Kinetics of disturbance forces and torques

The simulation accounts for magnetic disturbances and the gravity gradient as the vehicle falls to the earth, but does not account for drag disturbances. While drag would slow the vehicle, because the forces used remain constant, the DCM comparison remains valid.

3.2.4 Kinematics of motion

Preprints (www.preprints.org) | NOT PEER-REVIEWED | Posted: 28 February 2022 doi:10.20944/preprints202202.0360.v1

As discussed in Section 2, the only "true" Euler angle output from a DCM is the last mathematical rotation. For the purposes of analysis, the true Roll angle, Φ, is pulled from executing a 321 rotation; the true pitch angle, Θ, is from a 132 rotation; and the true yaw angle, ψ, is from a 213 rotation. The true Euler angles from these rotations is given as Φ = -0.5825°, Θ = 10.2404°, and ψ = 0.0863°. With the defined maneuver of Φ = 10°, Θ = -30°, and ψ = 30°, the desired angles, rates and acceleration trajectories remain constant.

Changing the mathematical rotation order changes the flightpath and distance traveled of the vehicle as displayed in Figure 4. Derived Euler angles with associated error and computational burden expressed in run time for each rotation are found in Table 2.

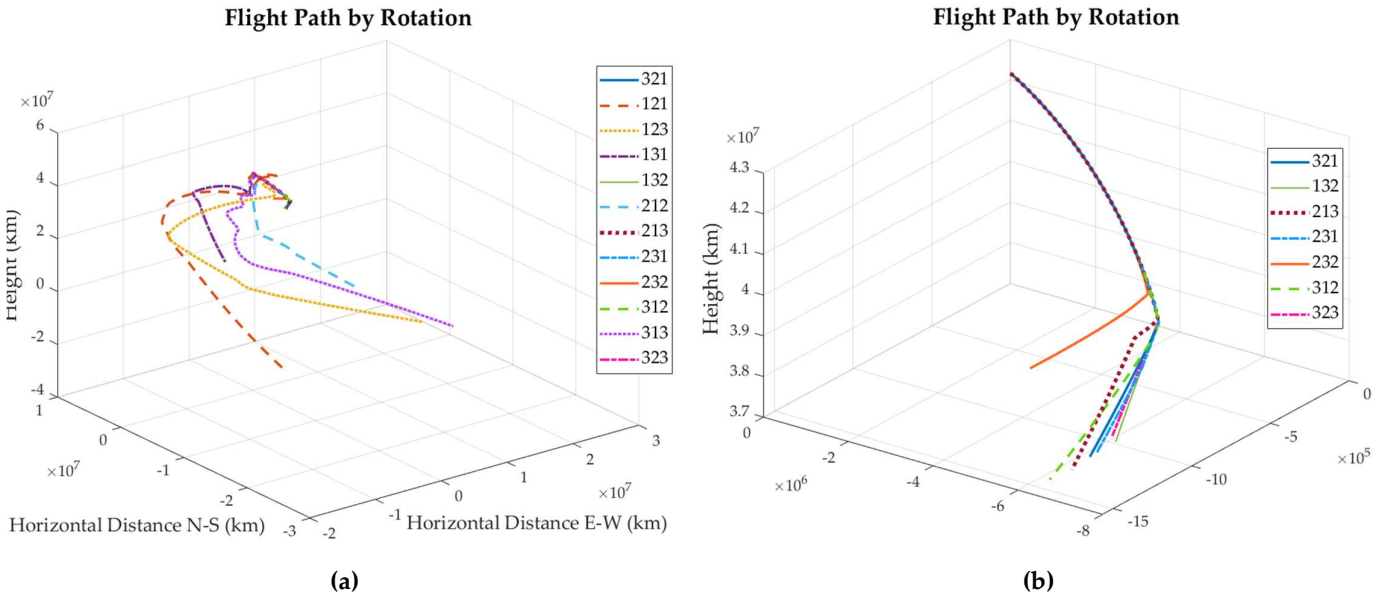

Figure 4. Three-dimensional flight path of the vehicle based on the order of mathematical rotation chosen in the DCM and a zoomed in portion on the rotations traveling closest to each other.

Table 2. Derived Euler Angles, Associated Error, and Simulation Run Time

Rotation	Angle	Derived Value (Deg)	Error (Deg)	Average Error (Deg)	Run Time (Sec)	Rotation	Angle	Derived Value (Deg)	Error (Deg)	Average Error (Deg)	Run Time (Sec)
	Roll (Φ)	130.7395	131.322				Roll (Φ)	0.4906	1.0731		
121	Pitch (Θ)	45.0	34.7596	55.3893	0.005	231	Pitch (Θ)	-10.2447	20.4851	7.312	0.014
	Yaw (ψ)	0.0	0.0863				Yaw (ψ)	-0.2915	0.3778		
	Roll (Φ)	144.7919	145.3744				Roll (Φ)	108.6987	109.2812		
123	Pitch (Θ)	-6.3093	16.5497	58.7043	0.014	232	Pitch (Θ)	0.0	10.2404	97.58703	0.013
	Yaw (ψ)	-14.1025	14.1888				Yaw (ψ)	-173.153	173.2395		
	Roll (Φ)	0.0	0.5825				Roll (Φ)	0.9839	1.5664		
131	Pitch (Θ)	-164.374	174.6144	108.4614	0.013	312	Pitch (Θ)	10.2398	0.0006	0.5805	0.014
	Yaw (ψ)	-150.101	150.1873				Yaw (ψ)	0.2608	0.1745		
	Roll (Φ)	-0.2011	0.3814				Roll (Φ)	0.0	0.5825		
132	Pitch (Θ)	10.2404	0.0	0.143967	0.013	313	Pitch (Θ)	-156.248	166.4886	89.83103	0.012
	Yaw (ψ)	0.1368	0.0505				Yaw (ψ)	-102.336	102.422		
	Roll (Φ)	76.5964	77.1789				Roll (Φ)	-0.5825	0.0		
212	Pitch (Θ)	-16.0803	26.3207	34.52863	0.012	321	Pitch (Θ)	-10.2373	20.4777	6.8473	0.015
	Yaw (ψ)	0.0	0.0863				Yaw (ψ)	0.1505	0.0642		

 doi:10.20944/preprints202202.0360.v1

	Roll (Φ)	-0.8559	0.2734				Roll (Φ)	9.9889	10.5714		
213	Pitch (Θ)	-10.2349	20.4753	6.916233	0.013	323	Pitch (Θ)	0.0	10.2404	37.2335	0.011
	Yaw (ψ)	0.0863	0.0				Yaw (ψ)	90.975	90.8887		

4. Discussion

Based on this analysis, it can be shown that the most accurate single DCM rotation method for a vehicle delivered from orbit is the 132 sequences. Of all the rotation schemes, the 132 is the only rotation resulting in less than 1 degree of error in all three Euler angle calculations from the true Euler angles derived. The next closest solution is the 312 sequence with the most accurate pitch value of any rotation not used to calculate the true value. In all simulations when a rotation is repeated (i.e., 131 or 313), the average error is drastically larger than the remaining rotation schemes. All simulations had similar computational burdens, with eleven of the twelve rotation schemes separated by three one-thousandths of a second. Between the two most accurate rotation schemes, the 132 rotation was one one-thousandth of a second quicker than the 312 (0.013 vs 0.014 seconds). Therefore, in order to maximize accuracy for this type of weapon without increasing computing power required, a 132-rotation scheme will provide the most accurate solution, while any solution not rotating by one of the Euler angles will lead to the greatest miss.

Due to the construct of the simulation, the DCM was continuously updated as the vehicle fell to the ground, causing an updated Euler angle. While the method of solving for each angle resulted in no quadrant ambiguity, the angles values were dependent on other "non-true" values from the DCM sequence selected. In order to find a constant true Euler angle, further research can be conducted to resolve this dependency.

Funding: This research received no external funding. The APC was funded by the corresponding author.

Data Availability Statement: Data may be made available by contacting the corresponding author.

Acknowledgments: I would like to thank Prof. Timothy Sands for the technical background found in section two and assistance in troubleshooting Matlab and Simulink code.

Conflicts of Interest: The authors declare no conflict of interest.

References

1. Euler, L. (Euler) Formulae Generales pro Translatione Quacunque Corporum Rigidorum (General Formulas for the Translation of Arbitrary Rigid Bodies), Presented to the St. Petersburg Academy on 9 October 1775. and First Published in *Novi Commentarii Academiae Scientiarum Petropolitanae* 20, 1776, pp. 189–207 (E478) and Was Reprinted in *Theoria motus corporum rigidorum*, ed. nova, 1790, pp. 449–460 (E478a) and Later in His Collected Works Opera Omnia, Series 2, Volume 9, pp. 84–98. Available online: https://math.dartmouth.edu/~euler/docs/originals/E478.pdf (accessed on 24 October 2021).
2. Thompson, W.; Tait, P.G. *Elements of Natural Philosophy*; Cambridge University Press: Cambridge, UK, 1872.
3. Reuleaux, F.; Kennedy Alex, B.W. *The Kinematics of Machinery: Outlines of a Theory of Machines*; Macmillan: London, UK, 1876; Available online: https://archive.org/details/kinematicsofmach00reuluoft (accessed on 24 October 2021).
4. Wright, T.W. *Elements of Mechanics Including Kinematics, Kinetics and Statics*; D. Van Nostrand Company: New York, NY, USA; Harvard University: Cambridge, MA, USA, 1896.
5. Merz, J.T. *A History of European Thought in the Nineteenth Century*; Blackwood: London, UK, 1903; p. 5.
6. Whittaker, E.T. *A Treatise on the Analytical Dynamics of Particles and Rigid Bodies*; Cambridge University Press: Cambridge, UK, 1904.
7. Whittaker, E.T. *A Treatise on the Analytical Dynamics of Particles and Rigid Bodies*; Cambridge University Press: Cambridge, UK, 1917.
8. Whittaker, E.T. *A Treatise on the Analytical Dynamics of Particles and Rigid Bodies*; Cambridge University Press: Cambridge, UK, 1927.
9. Whittaker, E.T. *A Treatise on the Analytical Dynamics of Particles and Rigid Bodies*; Cambridge University Press: Cambridge, UK, 1937.
10. Church, I.P. *Mechanics of Engineering*; Wiley: New York, NY, USA, 1908; p. 111. [Google Scholar]
11. Wright, T.W. *Elements of Mechanics Including Kinematics, Kinetics, and Statics*, with Applications; Nostrand: New York, NY, USA, 1909.

12. Study, E. ; Delphenich, D.H., Translator; Foundations and goals of analytical kinematics. *Sitzber. d. Berl. Math. Ges.* **1913**, *13*, 36–60. Available online: http://neo-classical-physics.info/uploads/3/4/3/6/34363841/study-analytical_kinematics.pdf (accessed on 14 April 2017).
13. Gray, A. *A Treatise on Gyrostatics and Rotational Motion*; MacMillan: London, UK, 1918; ISBN 978-1-4212-5592-7. (Published 2007).
14. Truesdell C. The present status of the controversy regarding the bulk viscosity of fluids. *Proc. R. Soc.* **1954**. http://doi.org/10.1098/rspa.1954.0237
15. Fox, G. Methods for Constructing Invariant Amplitudes Free from Kinematic Singularities and Zeros. *Phys. Rev.* **1967**, 157, 1493.
16. Rose, M.E. *Elementary Theory of Angular Momentum*; John Wiley & Sons: New York, NY, USA, 1957; ISBN 978-0-486-68480-2. (Published 1995).
17. Kane, T.R. *Analytical Elements of Mechanics Volume 1*; Academic Press: New York, NY, USA; London, UK, 1959.
18. Kane, T.R. *Analytical Elements of Mechanics Volume 2 Dynamics*; Academic Press: New York, NY, USA; London, UK, 1961.
19. Fang, A.C.; Zimmerman, B.G. *Digital Simulation of Rotational Kinematics*; NASA Technical Report NASA TN D-5302; NASA: Washington, DC, USA, October 1969. Available online: https://ntrs.nasa.gov/archive/nasa/casi.ntrs.nasa.gov/19690029793.pdf (accessed on 24 October 2021).
20. Henderson, D.M. *Euler Angles, Quaternions, and Transformation Matrices*—Working Relationships; As NASA Technical Report NASA-TM-74839; July 1977. Available online: https://ntrs.nasa.gov/archive/nasa/casi.ntrs.nasa.gov/19770024290.pdf (accessed on 24 October 2021).
21. Henderson, D.M. *Euler Angles, Quaternions, and Transformation Matrices for Space Shuttle Analysis*; Houston Astronautics Division as NASA Design Note 1.4-8-020; 9 June 1977. Available online: https://ntrs.nasa.gov/archive/nasa/casi.ntrs.nasa.gov/19770019231.pdf (accessed on 24 October 2021).
22. Smeresky, B.; Rizzo, A.; Sands, T. Kinematics in the Information Age. *Mathematics* **2018**, *6*(9), 148. https://doi.org/10.3390/math6090148
23. Conversion between quaternions and Euler angles. Available online: https://en.wikipedia.org/wiki/Conversion_between_quaternions_and_Euler_angles (accessed on 18 Aug 2021).
24. Quaternions and spatial rotation. Available online: https://en.wikipedia.org/wiki/Quaternions_and_spatial_rotation#Quaternion-derived_rotation_matrix (accessed on 16 Aug 2021).

Preprints (www.preprints.org) | NOT PEER-REVIEWED | Posted: 28 February 2022 doi:10.20944/preprints202202.0360.v1

Appendix A Complete display of all SIMULINK systems and subsystems

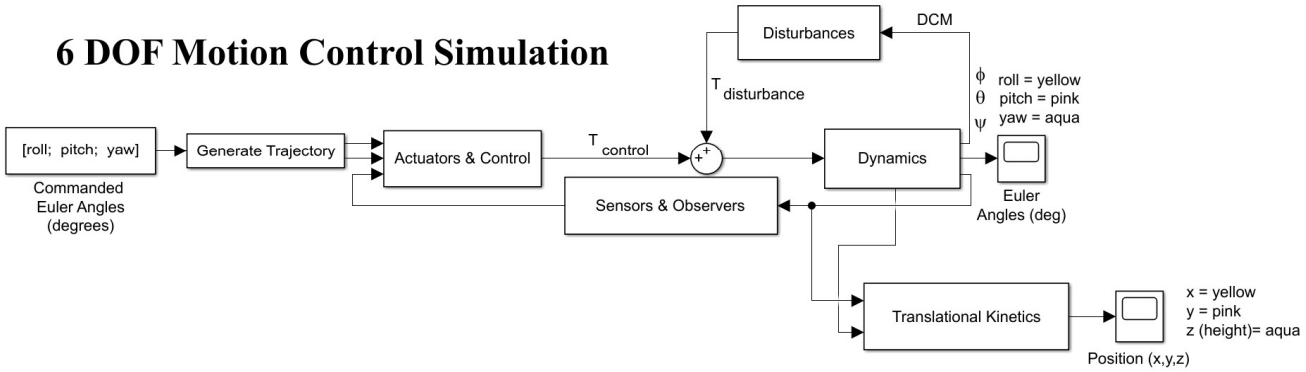

Figure A1. Simulink System Page

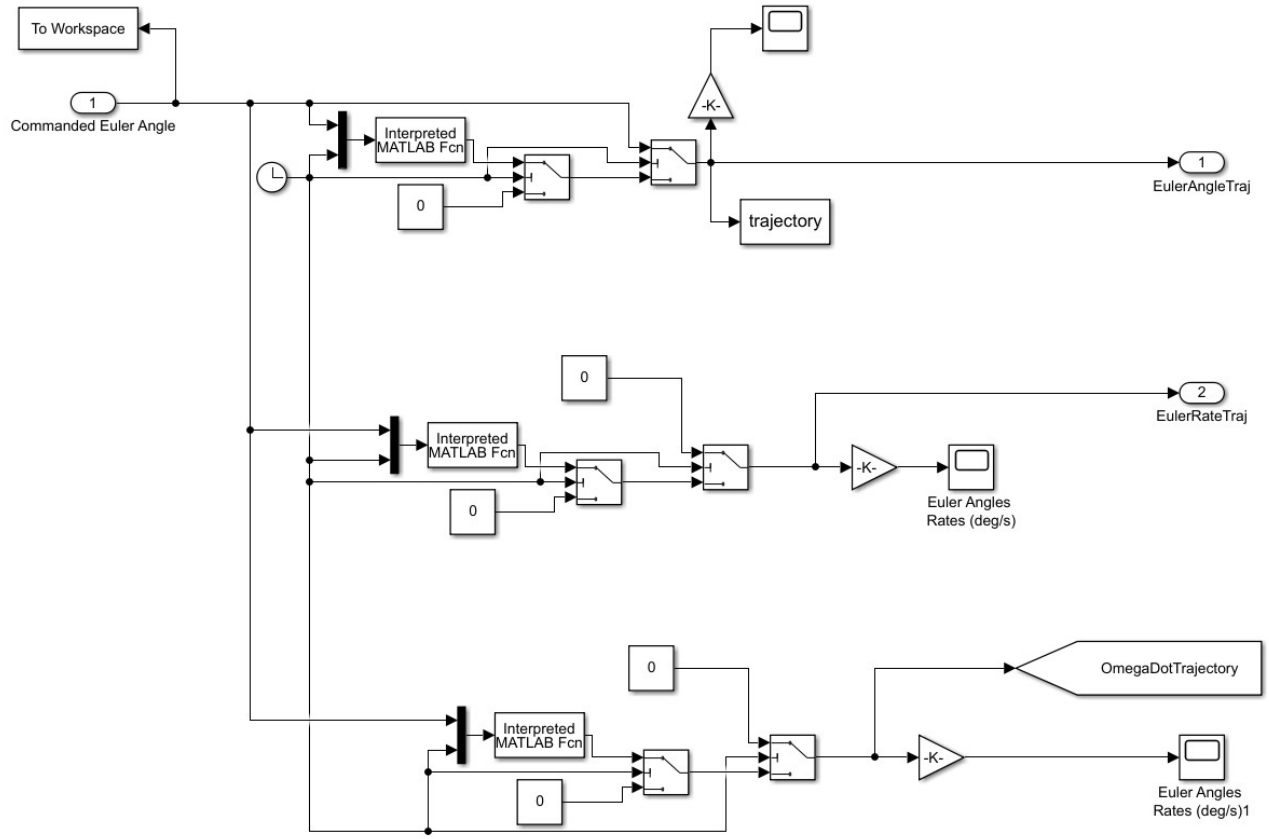

Figure A2. Trajectory Generation Subsystem

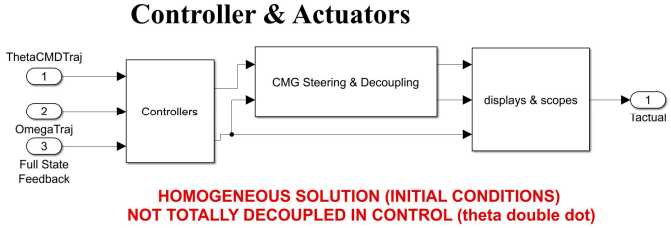

Preprints (www.preprints.org) | NOT PEER-REVIEWED | Posted: 28 February 2022 doi:10.20944/preprints202202.0360.v1

Figure A3. Actuators and Controls Subsystem

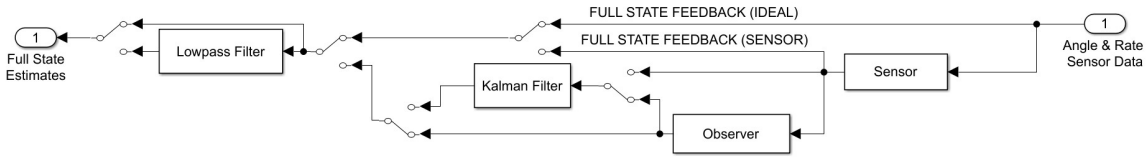

Figure A4. Sensors and Observers Subsystem

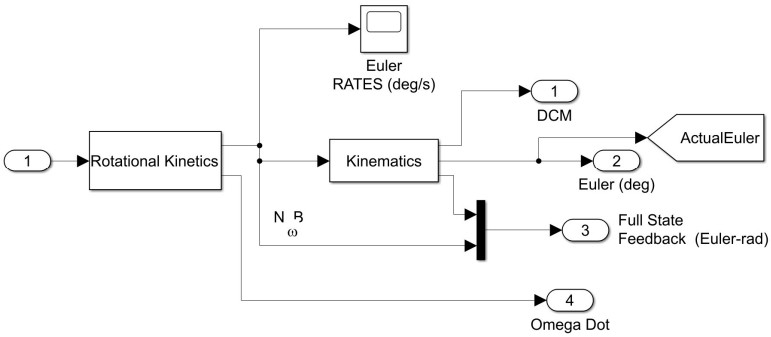

Figure A5. Dynamics Subsystem

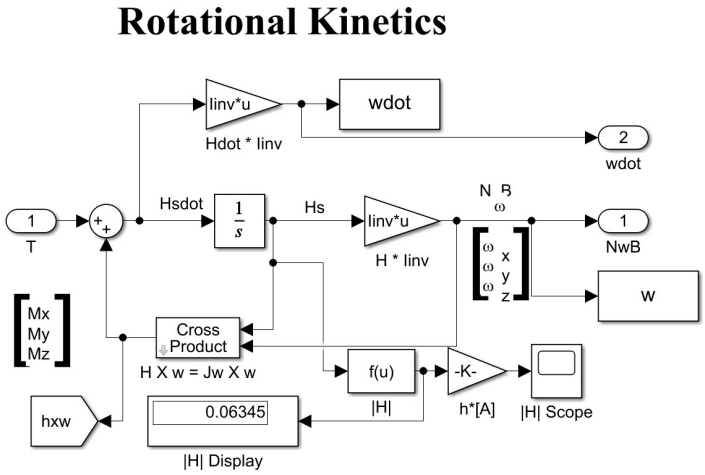

Figure A6. Rotational Kinetics Subsystem

Preprints (www.preprints.org) | NOT PEER-REVIEWED | Posted: 28 February 2022 doi:10.20944/preprints202202.0360.v1

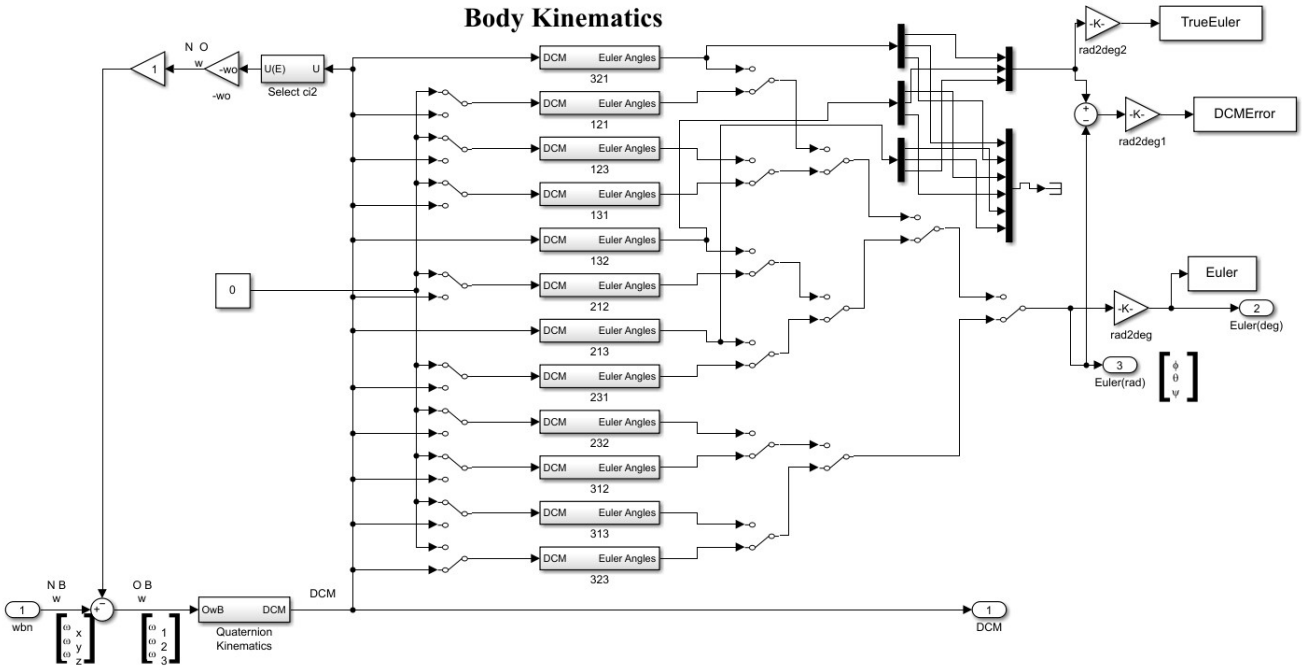

Figure A7. Kinematics Subsystem

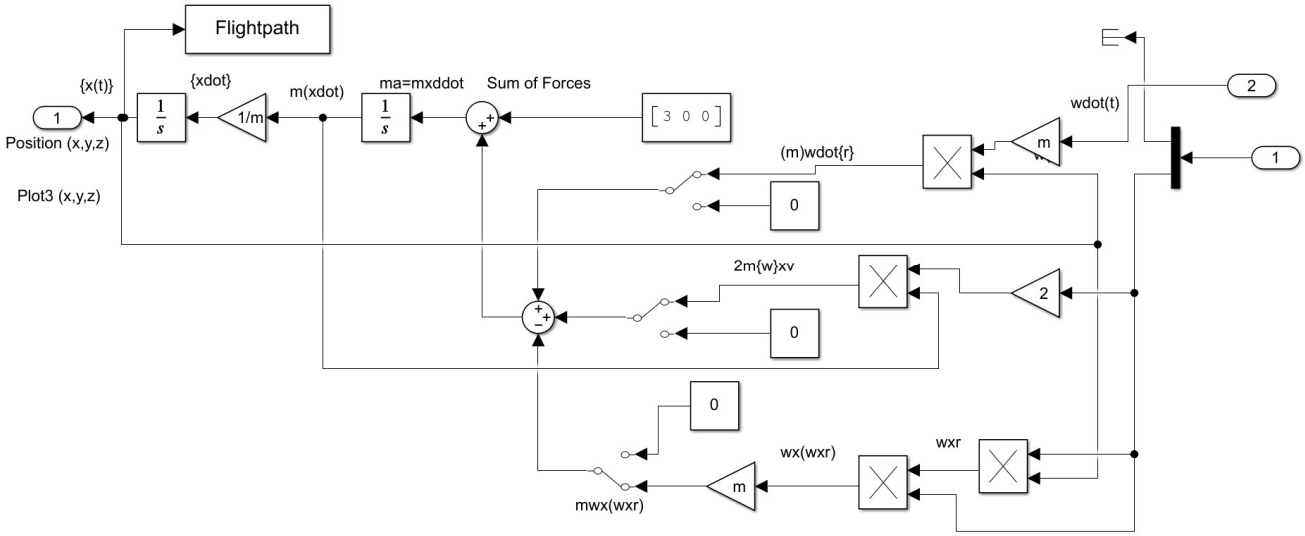

Figure A8. Translational Kinetics Subsystem

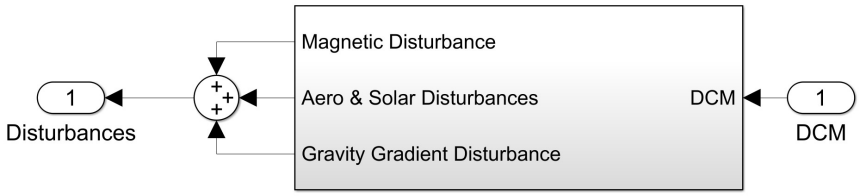

Figure A9. Disturbances Summing Subsystem

Preprints (www.preprints.org) | NOT PEER-REVIEWED | Posted: 28 February 2022 doi:10.20944/preprints202202.0360.v1

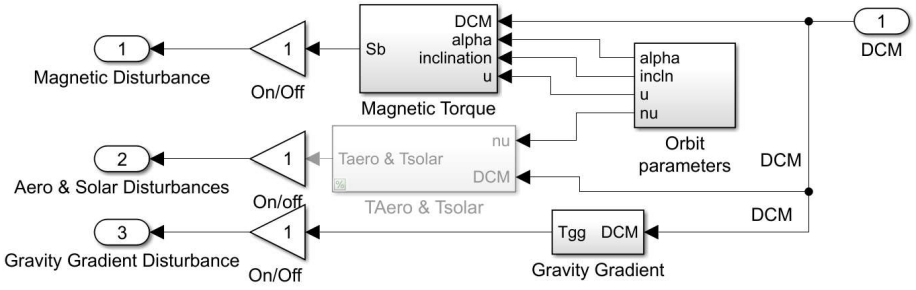

Figure A10. Disturbances Subsystem

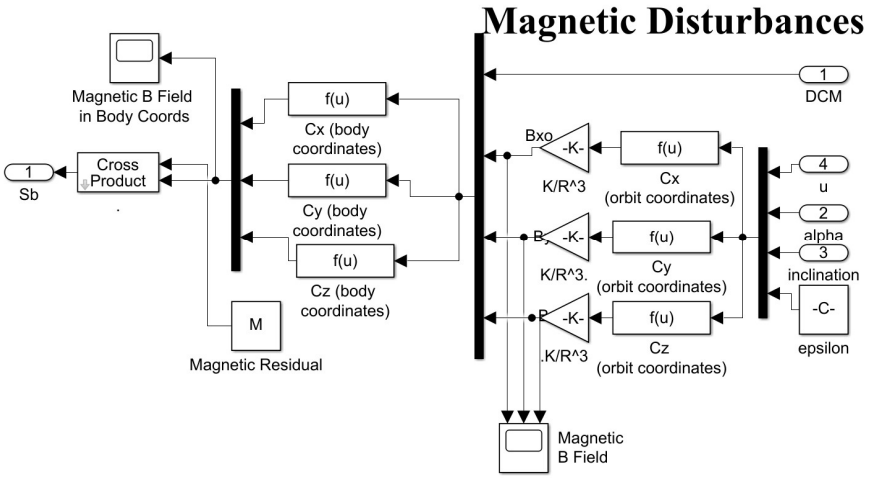

Figure A11. Magnetic Disturbances Subsystem

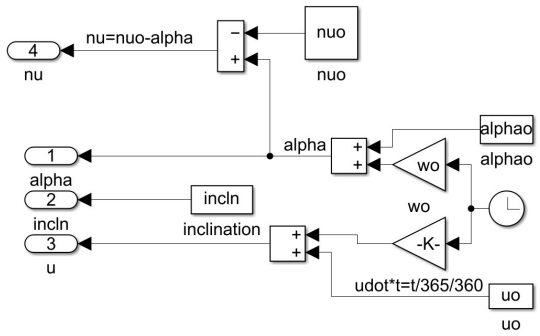

Figure A12. Orbit Parameters Subsystem

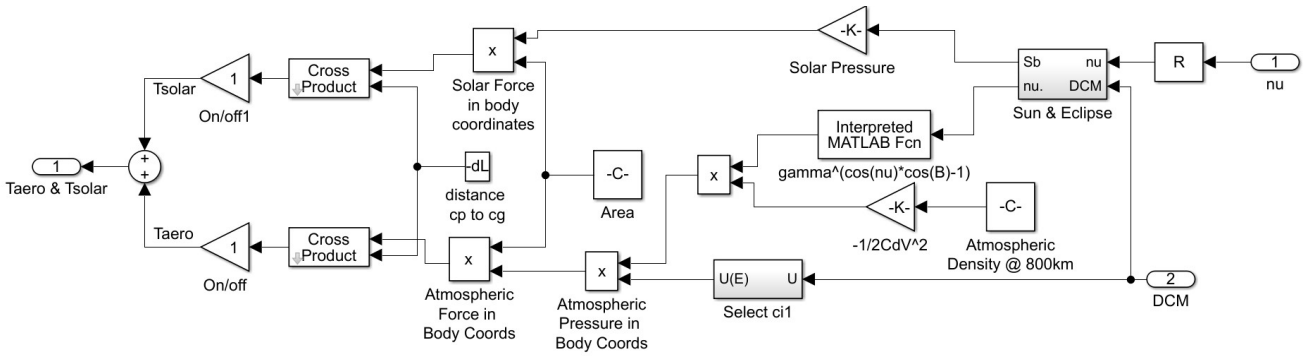

Figure A13. Solar and Aero Disturbances Subsystem

 doi:10.20944/preprints202202.0360.v1

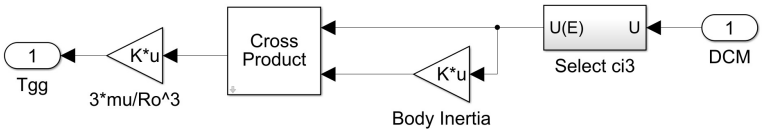

Figure A14. Gravity Gradient Subsystem

Appendix B Complete MATLAB codes usable to duplicate results in this manuscript